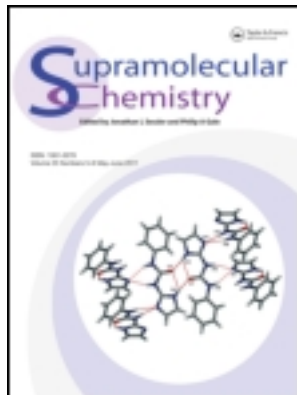


This article was downloaded by: [McGill University Library]

On: 19 October 2012, At: 02:28

Publisher: Taylor & Francis

Informa Ltd Registered in England and Wales Registered Number: 1072954 Registered office: Mortimer House, 37-41 Mortimer Street, London W1T 3JH, UK



Supramolecular Chemistry

Publication details, including instructions for authors and subscription information:

<http://www.tandfonline.com/loi/gsch20>

Supramolecular architecture of picric acid and pyrazoles: syntheses, structural, computational and thermal studies

Udai P. Singh^a, Nidhi Goel^a, Gurdip Singh^b & Pratibha Srivastava^b

^a Department of Chemistry, Indian Institute of Technology Roorkee, Roorkee, 247 667, India

^b Department of Chemistry, DDU Gorakhpur University, Gorakhpur, 273000, India

Version of record first published: 23 Apr 2012.

To cite this article: Udai P. Singh, Nidhi Goel, Gurdip Singh & Pratibha Srivastava (2012): Supramolecular architecture of picric acid and pyrazoles: syntheses, structural, computational and thermal studies, *Supramolecular Chemistry*, 24:4, 285-297

To link to this article: <http://dx.doi.org/10.1080/10610278.2012.655276>

PLEASE SCROLL DOWN FOR ARTICLE

Full terms and conditions of use: <http://www.tandfonline.com/page/terms-and-conditions>

This article may be used for research, teaching, and private study purposes. Any substantial or systematic reproduction, redistribution, reselling, loan, sub-licensing, systematic supply, or distribution in any form to anyone is expressly forbidden.

The publisher does not give any warranty express or implied or make any representation that the contents will be complete or accurate or up to date. The accuracy of any instructions, formulae, and drug doses should be independently verified with primary sources. The publisher shall not be liable for any loss, actions, claims, proceedings, demand, or costs or damages whatsoever or howsoever caused arising directly or indirectly in connection with or arising out of the use of this material.

Supramolecular architecture of picric acid and pyrazoles: syntheses, structural, computational and thermal studies

Udai P. Singh^{a*}, Nidhi Goel^a, Gurdip Singh^b and Pratibha Srivastava^b

^aDepartment of Chemistry, Indian Institute of Technology Roorkee, Roorkee 247 667, India; ^bDepartment of Chemistry, DDU Gorakhpur University, Gorakhpur 273000, India

(Received 28 September 2011; final version received 22 December 2011)

The salts comprised of picric acid [(OH)(NO₂)₃C₆H₂] and different ditopic pyrazoles Pz^{R₁,R₂}H (where R₁ = R₂ = H for **1**, R₁ = R₂ = Me for **2**, R₁ = Ph, R₂ = Me for **3**) and 3,3',5,5'-tetramethyl-4,4'-bipyrazole (Me₄bpz) **4** are reported. Due to presence of different substituents on pyrazole, each salt contains infinite three-dimensional structure held together by primary N–H···O, O–H···N, O–H···O hydrogen bonds and secondary C–H···O interactions. The structure and harmonic vibration frequencies of the complexes were calculated in terms of the density functional theory. The orientation of molecule remains same in both the solid phase and the gaseous phase. The thermal decomposition of these salts was studied by thermogravimetry and differential thermogravimetric analysis. Kinetic parameters were evaluated using model-fitting and isoconversional methods.

Keywords: picric acid; pyrazoles; hydrogen bond interaction energy; thermolysis; ignition delay

1. Introduction

In chemistry and material science, the role of molecule with different functional groups has become an important area of research (1–3). One can achieve materials with desired physical and chemical properties by using different functionalities in the building units (4, 5). Picric acid with three nitro groups forms crystalline picrates of various organic molecules through ionic, non-covalent and π – π interactions as these interactions have been widely utilised as a supramolecular heterosynthon in the design of co-crystals (6, 7). It is known that picric acid acts not only as an acceptor but also as an acidic ligand to form strong hydrogen bonds with nitrogen atoms in heteroaromatic rings (8). Bonding of electron donor/acceptor picric acid molecules strongly depends on the nature of secondary organic moieties. In the past, picric acid has been used for co-crystallisation (9–16) by several workers. However, the literature on co-crystallisation using pyrazole as one component and picric acid as other component is very limited (17–19). The pyrazole nucleus both thermally and hydrolytically is very stable and occupies a position similar to that of pyridine or ammonia in spectrochemical series. As a ligand, it coordinates to metals and metalloids through 2-N but after deprotonation, the formed pyrazolate anions can coordinate through both nitrogen atoms as an exobidentate ligand of C_{2v} symmetry. The nucleophilicity of the nitrogen and their steric accessibility may be varied through appropriate ring substitution. Due to these

attractive features, the pyrazole and its derivatives have been used for co-crystallisation with picric acid to see the effect of substituents present on pyrazole ring on supramolecular network and thermal stability of picric acid. The present paper reports the co-crystallisation of the picric acid and pyrazole synthons as well the thermolysis of these salts.

2. Experimental

2.1 Materials

All manipulations were performed in air using commercial grade solvents after pre-dried by appropriate drying agents (20). Picric acid (2,4,6-trinitrophenol), pyrazole (PzH) and 3,5-dimethylpyrazole (Pz^{Me₂}H) were purchased from Aldrich Chemical Company (St. Louis, MO, USA). 3-phenyl-5-methylpyrazole (Pz^{Ph,Me}H) and 3,3',5,5'-tetramethyl-4,4'-bipyrazole (Me₄bpz) were prepared by the methods available in the literature (21, 22).

2.2 Instrumentation

Crystallised salts were carefully dried under vacuum for several hours prior to elemental analysis on Elementar Vario EL III analyzer. IR spectra were obtained on a Thermo Nicolet Nexus FT-IR spectrometer in KBr. ¹H and ¹³C NMR spectra were recorded on Bruker-D-Avance 500 spectrometer with Fourier transform technique using

*Corresponding author. Email: udaipfcy@iitr.ernet.in

tetramethylsilane as internal standard. The melting points were determined on a JSGW melting point apparatus.

2.2.1 X-ray crystallography

The X-ray data collection was performed on a Bruker Kappa Apex four-circle CCD diffractometer using graphite-monochromated MoK α radiation ($\lambda = 0.71070 \text{ \AA}$) at 100 K. In the reduction of data Lorentz and polarisation corrections, empirical absorption corrections were applied (23). Crystal structures were solved by direct methods. Structure solution, refinement and data output were carried out with the SHELXTL program (24, 25). Non-hydrogen atoms were refined anisotropically. Hydrogen atoms were placed in geometrically calculated positions by using a riding model. Images and hydrogen bonding interactions were created in the crystal lattice with DIAMOND and MERCURY software (26, 27).

2.2.2 Computational study

Geometry optimisation of different species involved during the course of present investigation was done using density functional methods with 6-31G(d,p) basis set, with Gaussian 03 suite of program (28, 29). The input for the simulation was the Z-matrix generalised by Gaussian view that was also used for visualising the molecules with optimised geometries. The frequency calculation was also performed.

2.2.3 Thermal analysis

2.2.3.1 Non-isothermal thermogravimetry. Non-isothermal thermogravimetry (TG) of salts **1–4** was recorded in the temperature range 10–800°C at a heating rate of 10°C min⁻¹ in static air using PerkinElmer's (Pyris Diamond) (Woodland, California, USA) thermogravimetric analyzer. The accuracy of the furnace was $\pm 1^\circ\text{C}$.

2.2.3.2 Isothermal TG. The isothermal TG studies (wt 0.033 g, 100–200 mesh) of salts **1–4** were also performed at appropriate temperatures (200–240°C) in static air using indigenously fabricated TG apparatus (30) fitted with temperature cum controller.

2.2.3.3 Ignition delay measurements. The ignition delay (D_i) data were recorded using tube furnace technique (31) (mass 0.020 g, 100–200 mesh) in the temperature range 340–380°C ($\pm 1^\circ\text{C}$). Each run was repeated five times and the mean D_i values are calculated. The D_i data were found to fit in the following equation (32–34):

$$D_i = Ae^{E_a^*/RT},$$

where E_a^* is the activation energy for thermal ignition, A is the pre-exponential factor and T is the absolute temperature. E_a^* was determined from the slope of a plot of $\ln(D_i)$ versus $1/T$.

2.2.3.4 Percent oxygen balance. The percent oxygen balance (OB) was calculated by following equation suggested by Martin and Yallop (35):

$$\text{OB} = \frac{[(z - 2x - (y/2))]100}{n},$$

where x , y and z are the respective number of atoms of C, H, N, respectively, and n is the total number of atoms in the molecule.

2.2.4 Kinetics analysis of isothermal TG data

Kinetic analysis of solid state decomposition is usually based on a single-step kinetic equation (36):

$$\frac{d\alpha}{dt} = k(T)f(\alpha), \quad (1)$$

where t is the time, T is the temperature, α is the extent of conversion ($0 < \alpha < 1$), $k(T)$ is the rate constant and $f(\alpha)$ is the reaction model (37), which describes the dependence of the reaction rate on the extent of reactions. The value of α is experimentally derived from the global mass loss in TG experiments. The reaction model may take various forms; the temperature dependence of $k(T)$ can be satisfactorily described by the Arrhenius equation, whose substitution into equation (1) yields

$$\frac{d\alpha}{dt} = A \exp\left(\frac{-E}{RT}\right) \cdot f(\alpha), \quad (2)$$

where A is pre-exponential factor, E is activation energy and R is the gas constant.

2.2.4.1 Model-fitting method. Rearrangement and integration of equation (1) for isothermal conditions give

$$g_j(\alpha) = k_j(T)t, \quad (3)$$

where $g(\alpha) = \int_0^\alpha [f(\alpha)]^{-1} d\alpha$ is the integrated form of the reaction model. The subscript j has been introduced to emphasise that substituting a particular reaction model in equation (3) results in the evaluation of the corresponding rate constant, which is determined from the slope of a plot of $g_j(\alpha)$ versus t . For each reaction model selected, the rate constants are evaluated at several temperatures T_i and Arrhenius parameters are determined using the Arrhenius

equation (4) in its logarithmic form:

$$\ln k_j(T_i) = \ln A_j - \frac{E_j}{RT_i} \quad (4)$$

Arrhenius parameters were evaluated for isothermal experimental data by the model-fitting method.

2.2.4.2 Isoconversional method. This method allows the activation energy to be evaluated without making any assumptions about the reaction model. Additionally, the method evaluates the effective activation energy as a function of the extent of conversion which allows one to explore multistep kinetics.

The basic assumption of the isoconversional method (40) is that the reaction model as defined in equation (1) is not dependent on temperature or heating rate. Under isothermal conditions, on combining equations (3) and (4), we get

$$-\ln t_{\alpha,i} = \ln \left[\frac{A_\alpha}{g(\alpha)} \right] - \frac{E_\alpha}{RT_i} \quad (5)$$

where E_α is evaluated from the slope of the plot of $-\ln t_{\alpha,i}$ against T_i^{-1} . Thus, E_α at various α_i for salts **1–4** was evaluated.

2.3 Syntheses of organic salts

2.3.1 Synthesis of $[2PA^- \cdot 2PzH_2^+ \cdot OH_2] (1)$

Picric acid (0.22 g, 1.0 mmol) and pyrazole (0.06 g, 1.0 mmol) were mixed in a water–methanol mixture (v/v%, 1:4, 10 ml). The resulting solution was stirred for 6 h and filtered through celite. The filtrate was evaporated to dryness under vacuum and the yellow solid obtained was redissolved in methanol. The yellow crystals of salt **1** in 69.0% (0.42 g, 0.69 mmol) yield, suitable for X-ray data collection, were obtained by slow evaporation of solvent at room temperature. Anal. Calcd (%) for $C_{18}H_{16}N_{10}O_{15}$ (612.41): C, 76.49; H, 2.37; N, 23.56. Found: C, 76.35; H, 2.31; N, 23.47. IR (KBr, cm^{-1}): 3218, 3141, 2996, 1843, 1611, 1567, 1539, 1494, 1360, 1321, 1278, 1162, 1134, 1077, 909, 769, 711, 608, 543. 1H NMR (DMSO- d_6) δ : 8.48 (s, 2H, PA^-), 7.61 (t, 1H, pz), 6.26 (d, 2H, pz), 12.64 (s, br, 2H, NH). ^{13}C NMR (DMSO- d_6) δ : 159.61, 140.95, 133.15, 126.56, 125.17, 104.21. m.p. 130°C.

2.3.2 Synthesis of $[PA^- \cdot Pz^{Me_2}H_2^+] (2)$

Salt **2** was prepared by same procedure as outlined above for **1** using 3,5-dimethylpyrazole (0.09 g, 1.0 mmol) in methanol (10 ml) with 63.2% (0.20 g, 0.63 mmol) yield. Anal. Calcd (%) for $C_{11}H_{11}N_5O_7$ (325.25): C, 40.62; H,

3.40; N, 21.53. Found: C, 40.43; H, 3.29; N, 21.39. IR (KBr, cm^{-1}): 3191, 3126, 1576, 1469, 1336, 1298, 1154, 1032, 1008, 835, 737. 1H NMR (DMSO- d_6) δ : 8.49 (s, 2H, PA^-), 5.74 (s, 1H, pz), 2.12 (s, 6H, CH_3), 12.03 (s, br, 2H, NH). ^{13}C NMR (DMSO- d_6) δ : 159.59, 140.94, 144.68, 126.53, 125.15, 103.18, 11.85. m.p. 155°C.

2.3.3 Synthesis of $[PA^- \cdot Pz^{Ph,Me}H_2^+ \cdot CH_3OH] (3)$

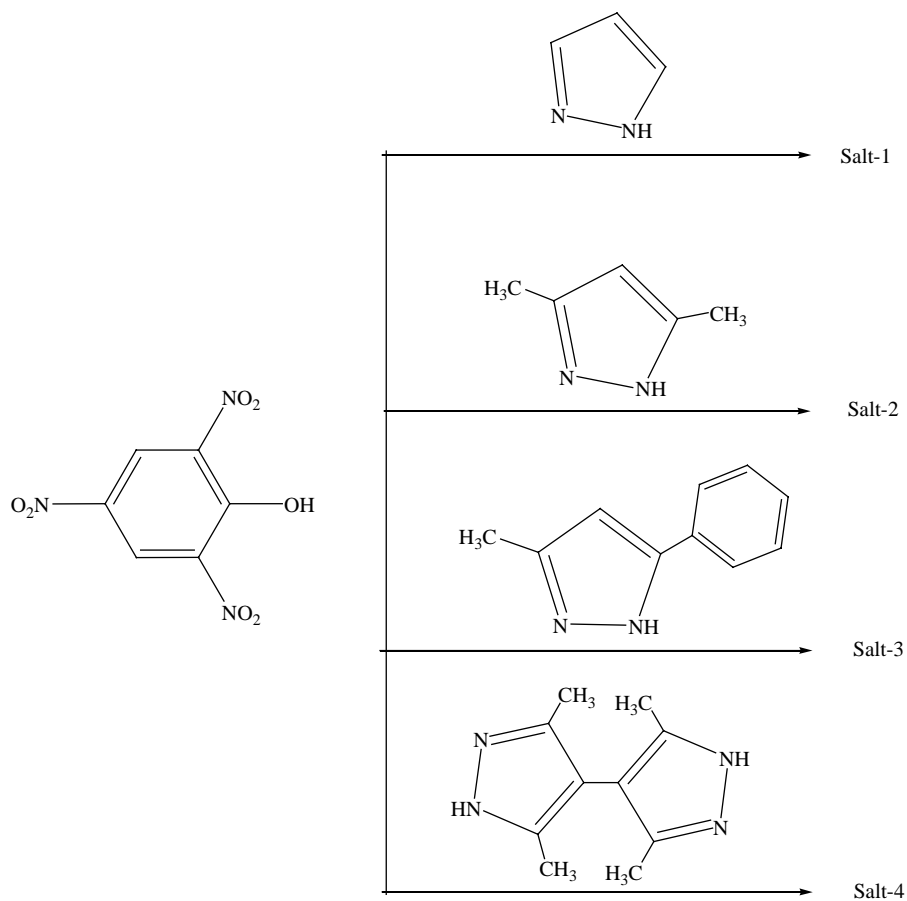
Salt **3** was prepared by same procedure as outlined above for **1** using 3-phenyl-5-methylpyrazole (0.16 g, 1.0 mmol) in methanol (10 ml) with 71.8% (0.30 g, 0.72 mmol) yield. Anal. Calcd (%) for $C_{17}H_{17}N_5O_8$ (419.36): C, 48.69; H, 4.08; N, 16.70. Found: C, 48.49; H, 3.97; N, 16.53. IR (KBr, cm^{-1}): 3308, 3102, 1860, 1627, 1533, 1431, 1341, 1260, 1151, 1082, 834, 780, 702, 534. 1H NMR (DMSO- d_6) δ : 8.48 (s, 2H, PA^-), 6.44 (s, 1H, pz), 2.25 (s, 3H, CH_3), 7.26–7.75 (m, 5H, Ph), 12.39 (s, br, 2H, NH), 3.16 (s, 3H, OCH_3). ^{13}C NMR (DMSO- d_6) δ : 159.60, 140.93, 126.57, 125.16, 148.21, 141.02, 133.93, 128.60, 127.24, 124.91, 100.19, 48.59, 11.04. m.p. 120°C.

2.3.4 Synthesis of $[2PA^- \cdot 2Me_4bpzH^+ \cdot CH_3CN] (4)$

Salt **4** was prepared by same procedure as outlined above for **1** using 3,3',5,5'-tetramethyl-4,4'-bipyrazole (0.19 g, 1.0 mmol) in an acetonitrile–methanol mixture (v/v%, 1:4, 10 ml) with 68.9% (0.61 g, 0.68 mmol) yield. Anal. Calcd (%) for $C_{34}H_{37}N_{15}O_{14}$ (879.79): C, 46.41; H, 4.23; N, 23.88. Found: C, 46.37; H, 4.19; N, 23.73. IR (KBr, cm^{-1}): 3347, 1830, 1626, 1581, 1536, 1426, 1313, 1165, 1072, 907, 812, 710, 616. 1H NMR (DMSO- d_6) δ : 8.46 (s, 2H, PA^-), 1.95 (s, 12H, CH_3), 12.20 (s, br, 3H, NH), 2.07 (s, 3H, CH_3CN). ^{13}C NMR (DMSO- d_6) δ : 159.58, 148.30, 140.92, 137.37, 126.54, 125.21, 125.14, 120.99, 117.91, 66.68, 54.04, 1.03. m.p. 180°C.

3. Results and discussions

The reaction of picric acid and corresponding pyrazoles ($PzH/Pz^{Me_2}H/Pz^{Ph,Me}H/Me_4bpz$) in appropriate mixture of solvent resulted in the formation of ionic salts (**1–4**) as shown in Scheme 1. The different formulations for ionic salts **1–4** were confirmed by elemental analysis, IR, NMR and crystallographic structure analyses. The asymmetric and the symmetric stretching vibrations of $-NO_2$ group show bands at 1536 and 1334 cm^{-1} , respectively (11, 38). The shift of the $\nu_{as}(NO_2)$ vibration to lower frequency (1581–1530 cm^{-1}) in the spectrum of salts (**1–4**) compared with the free picric acid (1607 cm^{-1}) suggested the large electron density on the picric acid. The NH stretching vibration is normally observed at 3500–3400 cm^{-1} which is shifted to lower wave number due to the attraction of the $-NH$ protons by the picrate anion



Scheme 1. General method for preparation of salts **1–4**.

leading to an increase in —NH bond length in salts (**1–4**) (39). The shifting towards lower frequency in both cases is due to the hydrogen-bonded non-covalent interactions between donor (—NH protons) and acceptor (picrate anion) (40). The crystallographic and the selected hydrogen bonding data are given in Tables 1 and 2, respectively.

3.1 Structure description

3.1.1 Crystal structure of $[2\text{PA}^- \cdot 2\text{PzH}_2^+ \cdot \text{OH}_2]$ (**1**)

The salt **1** crystallises in the triclinic crystal system with P-1 space group. As shown in Figure 1, the unit cell consists of two molecules of protonated pyrazole with four NH group, two molecules of deprotonated picric acid (i.e. the acidic hydrogen of the hydroxyl group on picric acid has been transferred to the nitrogen atom of the pyrazole) and a water molecule. Both deprotonated OH groups of picric acid and protonated nitrogen atoms of both pyrazole molecules form a cationic–anionic acid–base pair via $\text{N—H} \cdots \text{O}$ [N7–H7A \cdots O1, 1.852(23) Å; N10–H10A \cdots O8, 1.930(21) Å] and $\text{C—H} \cdots \text{O}$ [C13–H13A \cdots O2, 2.581(1) Å; C18–H18 \cdots O9, 2.532(1) Å] intermolecular interactions

(Figure S1, available online). Due to the presence of various interactions, picrate and pyrazolate ions are self-assembled in a 3D square-shaped channels and these channels act as host molecules for water. The guest molecules (water) are situated between the two channels through $\text{N—H} \cdots \text{O}$ [N8–H8A \cdots O15, 1.783(24) Å; N9–H9B \cdots O15, 1.921(19) Å] as well as $\text{O—H} \cdots \text{O}$ [O15–H15A \cdots O8, 1.969(24); O15–H15A \cdots O14, 2.259(22) Å; O15–H16A \cdots O1, 2.037(23) Å] non-covalent interactions (Figure 2).

3.1.2 Crystal structure of $[\text{PA}^- \cdot \text{Pz}^{\text{Me}2}\text{H}_2^+]$ (**2**)

The unit cell of **2** contains one molecule of anionic deprotonated picric acid and one molecule of cationic protonated 3,5-dimethylpyrazole (Figure 3). It also crystallises in the triclinic crystal system with P-1 space group and contains $\text{N—H} \cdots \text{O}$ [N4–H4A \cdots O1, 1.678(21) Å; N4–H4A \cdots O7, 2.298(24) Å; N5–H5 \cdots O7, 2.362(4) Å] as well as $\text{C—H} \cdots \text{O}$ [C2–H2 \cdots O6, 2.603(2) Å; C7–H7A \cdots O1, 2.606(3) Å; C9–H9 \cdots O4, 2.639(4) Å; C11–H11B \cdots O5, 2.478(4) Å] non-covalent interactions which are responsible for the formation of

Table 1. Crystal data and structure refinement parameters of salts **1–4**.

Salts	(1)	(2)	(3)	(4)
Formula	C ₁₈ H ₁₆ N ₁₀ O ₁₅	C ₁₁ H ₁₁ N ₅ O ₇	C ₁₇ H ₁₇ N ₅ O ₈	C ₃₄ H ₃₇ N ₁₅ O ₁₄
Formula weight	612.41	325.25	419.36	879.79
Crystal system	Triclinic	Triclinic	Monoclinic	Monoclinic
Space group	P-1	P-1	P 21/c	P 21/c
a (Å)	7.6790(2)	7.8020(3)	14.7308(10)	16.076(2)
b (Å)	11.8274(2)	8.2452(3)	7.0891(5)	21.176(3)
c (Å)	13.5296(3)	10.9454(4)	17.5439(12)	11.5913(15)
α (°)	98.5490(10)	101.136(2)	90	90
β (°)	101.7860(10)	92.809(3)	93.955(3)	94.078(7)
γ (°)	91.8420(10)	90.568(2)	90	90
V(Å ³)	1187.04(5)	689.89(4)	1827.7(2)	3935.9(9)
Z	2	2	4	4
Crystal habit	Square	Block	Block	Needle
Temperature	296(2)	296(2)	296(2)	296(2)
D _{calc} (g/cm ³)	1.713	1.566	1.524	1.485
μ(MoKα) (cm ⁻¹)	0.152	0.133	0.123	0.118
F(000)	628	336	872	1832
Crystal size	0.27 × 0.19 × 0.13	0.27 × 0.21 × 0.17	0.34 × 0.29 × 0.23	0.23 × 0.19 × 0.13
Theta for data collection (°)	1.56–30.93	2.52–31.85	1.39–28.26	1.27–28.40
No. of measured reflections	7439	4679	4457	9793
No. of observed reflections	6133	3140	3194	7226
Data/restraints/parameters	7439/0/412	4679/0/214	4457/0/282	9793/0/601
Goodness-of-fit	0.813	0.775	0.977	1.327
Final R indices [I > 2(I)]	R ₁ ^a wR ₂ ^b	0.0380 0.1383	0.0406 0.1163	0.0564 0.1843

^a $R_1 = \sum |F_o| - |F_c| / \sum |F_o|$.

^b $wR_2 = \{ \sum [w(F_o^2 - F_c^2)^2] / \sum w(F_o^2)^2 \}^{1/2}$.

sheet with rectangular cavities in 3D views (Figure 4(a), 4(b)). This cavity can be used for trapping the appropriate size of guest molecule (about 1.2 Å).

3.1.3 Crystal structure of [PA⁻·Pz^{Ph,Me}H₂⁺·CH₃OH] (3)

The co-crystallisation of picric acid and 3-phenyl-5-methylpyrazole resulted in the formation of salt **3** which crystallises in monoclinic system with P 1 21/c 1 space group. The methanol solvent present in lattice binds one molecule of picrate anion and one molecule of 3-phenyl-5-methylpyrazolate ion (Figure 5). The presence of different non-covalent interactions, viz. N—H···O [N1—H1···O1, 1.782(23) Å; N1—H1···O2, 2.315(21) Å; N2—H2A···O8, 1.664(22) Å], C—H···O [C1—H1C···O2, 2.355(2) Å; C6—H6···O7, 3.149(2) Å; C6—H6···O8, 2.859(2) Å; C7—H7···O7, 2.592(3) Å; C17—H17B···O5, 2.687(3) Å; C17—H17C···O6, 3.020(2) Å; C17—H17C···O7, 2.636(2) Å], O—H···O [O8—H8A···O1, 2.151(3) Å; O8—H8A···O6, 2.225(3) Å] cause the formation of host–guest structure (Figure S2, available online). Due to these interactions, cation and anion form the cross-wires which are stacked one above the other and form an oval-shaped cavity between the two sets of cross-wires for guest methanol molecule as shown in Figure 6.

3.1.4 Crystal structure of [2PA⁻·2Me₄bpzH⁺·CH₃CN] (4)

The salt **4** with two molecules of picric acid, two molecules of 3,3',5,5'-tetramethyl-4,4'-bipyrazole and one molecule of acetonitrile in unit cell crystallises in the monoclinic system with P 1 21/c space group (Figure 7). The N—H and C—H group of pyrazole in **4** is non-covalently interacted with O2, O8, O11, O13 and O14 atoms of picrate acceptor, forming a charge-assisted ⁺N—H···O⁻ [N13—H13A···O14, 2.792(25) Å; N14—H14A···O8, 1.800(25) Å; N14—H14A···O14, 2.284(25) Å] and ⁺C—H···O⁻ [C19—H19B···O11, 2.575(2) Å; C22—H22A···O11, 2.605(5) Å; C30—H30A···O2, 2.685(7) Å; C30—H30C···O5, 2.761(9) Å; C32—H32A···O8, 2.914(2) Å; C33—H33B···O14, 2.600(3) Å] hydrogen bonds. The presence of different non-covalent interactions resulted in the formation of host–guest structure where the host assembly was present with a rectangular-shaped cavity. This cavity is formed by the presence of various non-covalent interactions between the picrate and 3,3',5,5'-tetramethyl-4,4'-bipyrazolate ions. The guest acetonitriles are located inside the cavity through C—H···N [C2—H2···N15, 2.433(9) Å; C21—H21C···N15, 2.413(3) Å] intermolecular interactions where the solvent molecule behaves as both donor and acceptor (Figure S3, available online). All these interactions form the 3D zigzag railway tracks like perspective view (Figure 8).

Table 2. Non-covalent interactions for **1–4** (Å and °).

S. N	D—H...A	d(D—H)	d(H—A)	d(D—A)	<(DHA)>	
1.	[2PA ⁻ ·2PzH ₂ ⁺ ·OH ₂] (1)					
	O15-H16A...O1	0.847(22)	2.037(23)	2.804(2)	150.23(228)	
	O15-H16A...O7	0.847(22)	2.317(24)	2.904(2)	126.77(201)	
	O15-H15A...O8	0.831(25)	1.969(24)	2.721(2)	150.29(215)	
	O15-H15A...O14	0.831(25)	2.259(22)	2.837(2)	126.94(198)	
	N7-H7A...O1	0.877(22)	1.852(23)	2.693(2)	160.07(210)	
	N8-H8A...O15	0.920(24)	1.783(24)	2.679(2)	163.91(219)	
	N9-H9B...O15	0.869(19)	1.921(19)	2.724(2)	152.96(197)	
	N10-H10A...O8	0.851(22)	1.930(21)	2.764(2)	166.39(220)	
	2.	[PA ⁻ ·Pz ^{Me2} H ₂ ⁺] (2)				
N4-H4A...O1		0.954(21)	1.678(21)	2.596(4)	166.44(218)	
N4-H4A...O7		0.954(21)	2.298(24)	2.834(4)	114.87(162)	
N5-H5...O7		0.860(2)	2.362(4)	2.837(5)	115.19(9)	
C2-H2...O6		0.930(1)	2.603(2)	3.418(2)	146.62(8)	
C7-H7A...O1		0.960(2)	2.606(3)	3.374(5)	137.17(12)	
C9-H9...O4		0.930(2)	2.639(4)	3.516(6)	157.53(9)	
C11-H11B...O5		0.959(2)	2.478(4)	3.420(5)	167.26(12)	
3.		[PA ⁻ ·Pz ^{Ph,Me} H ₂ ⁺ ·CH ₃ OH] (3)				
		N1-H1...O1	0.912(23)	1.782(23)	2.647(4)	157.43(206)
	N1-H1...O2	0.912(23)	2.315(21)	2.888(4)	120.65(176)	
	N2-H2A...O8	1.014(22)	1.664(22)	2.660(3)	166.12(197)	
	O8-H8A...O1	0.820(1)	2.151(3)	2.846(4)	142.64(9)	
	O8-H8A...O6	0.820(1)	2.225(3)	2.900(3)	139.92(10)	
	C1-H1C...O2	0.960(2)	2.355(2)	3.170(3)	142.32(13)	
	C6-H6...O7	0.931(2)	3.149(2)	3.600(4)	111.83(12)	
	C6-H6...O8	0.929(2)	2.859(2)	3.728(4)	156.29(12)	
	C7-H7...O7	0.930(2)	2.592(3)	3.323(4)	135.81(13)	
	C17-H17B...O5	0.960(3)	2.687(3)	3.577(5)	154.55(14)	
	C17-H17C...O6	0.960(2)	3.020(2)	3.730(3)	131.81(14)	
	C17-H17C...O7	0.960(2)	2.636(2)	3.593(3)	174.87(14)	
4.	[2PA ⁻ ·2Me ₄ bpzH ⁺ ·CH ₃ CN] (4)					
	N13-H13A...O14	0.947(23)	2.792(25)	2.989(9)	143.64(22)	
	N14-H14A...O8	0.901(25)	1.800(25)	2.679(8)	164.75(227)	
	N14-H14A...O14	0.901(25)	2.284(25)	2.776(11)	114.67(34)	
	C2-H2...N15	0.930(2)	2.433(9)	3.193(11)	138.85(16)	
	C19-H9B...O11	0.960(2)	2.575(2)	3.471(3)	155.35(14)	
	C21-H21C...N15	0.960(3)	2.413(3)	3.240(4)	144.19(19)	
	C22-H22A...O11	0.960(2)	2.605(5)	3.491(5)	153.47(14)	
	C30-H30A...O2	0.960(3)	2.685(7)	3.349(11)	126.77(14)	
	C30-H30C...O5	0.960(4)	2.761(9)	3.592(13)	145.26(15)	
	C32-H32A...O8	0.960(4)	2.914(2)	3.649(6)	134.26(14)	
	C33-H33B...O14	0.959(4)	2.600(3)	3.331(6)	133.18(22)	

The above structural studies reveal that on increasing the substituents of pyrazole ring, the number of non-covalent interactions varies from salt **1** to **4**, which in turn causes different type of 3D packing view for each salt. The presence of vacant cavity in salt **2** may be used for trapping suitable size of cations/anions.

3.2 Computational study

The optimised structural parameters of all individual pyrazoles, acids and their salts were calculated at B3LYP/6-31G(d,p) basis sets and are summarised in Table S1 (available online). Each optimised geometries showed positive vibrational frequencies showing that

optimised structure was the global minimum on the potential energy surface. Single-point energy calculations were performed, and zero-point corrected total energies for various species were recorded. In addition to the characterisation of these salts, the gas phase geometries, harmonic vibrational frequencies and binding energies of a series of pyrazole and their substituted derivatives were computed. The B3LYP predicted structure of salts as shown in Figure 9 and geometrical parameters are given in Table S1 (available online).

The hydrogen bond interaction energies were determined according to the following equation:

$$\Delta E = E_{\text{salt}} - (E_{\text{pyrazole}} - E_{\text{acid}}),$$

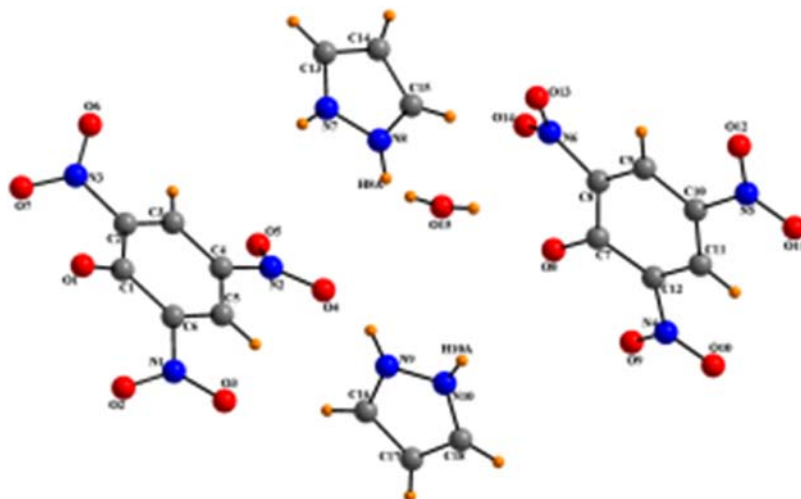


Figure 1. Molecular structure of salt **1**.

where E_{salt} , E_{pyrazole} and E_{acid} are the zero-point corrected total energies of salt, pyrazole and acid calculated at DFT(B3LYP)/6-31G(d,p) level of theory. We have removed the solvent and water molecules to check the relative stability.

The trend observed for the hydrogen bond interaction energy is given in Table 3. In case of salts **1** and **2**, the number of non-covalent interactions are same as both have almost same amount of hydrogen bond interaction energy. On the other hand, in salts **3** and **4**, the interaction

energy is still greater than **1** and **2** as the number of non-covalent interactions are high but the steric hindrance of pyrazole also plays an important role. The more steric hindered groups on the pyrazole ring reduce the hydrogen bond interaction energy. This is important to point out that the salt **3** shows the more hydrogen bond interaction energy than salt **4** due to the fact that the two pyrazole rings create the much more steric hindrance in salt **4** as compared to salt **3** which reduces the hydrogen bond interaction energy. Along with this, the negligible difference in the energy of the optimised structure of

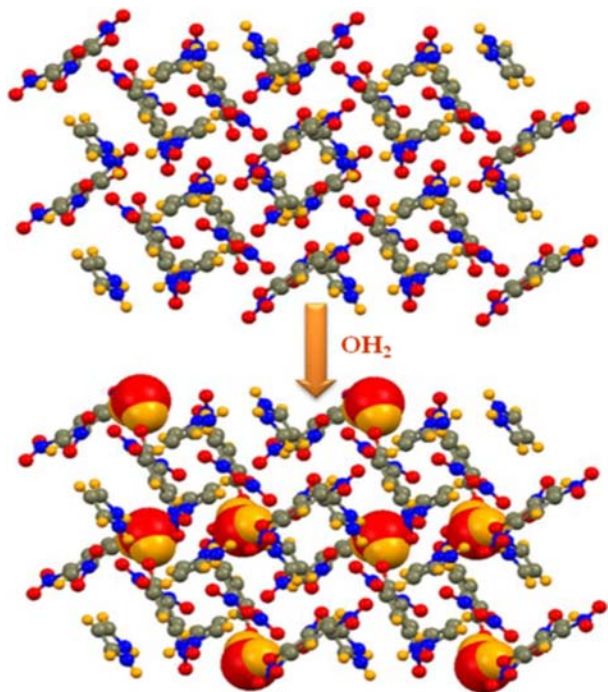


Figure 2. Host-guest complex formed due to N—H···O, C—H···O, O—H···O intermolecular interactions in salt **1**. (The H₂O molecules occupying the cavity as guest molecules between the alternate channels are represented in space-fill model).

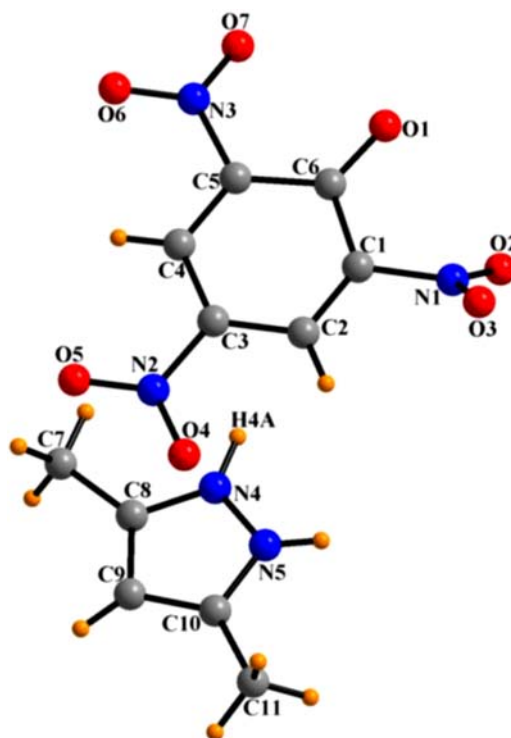


Figure 3. Molecular structure of salt **2**.

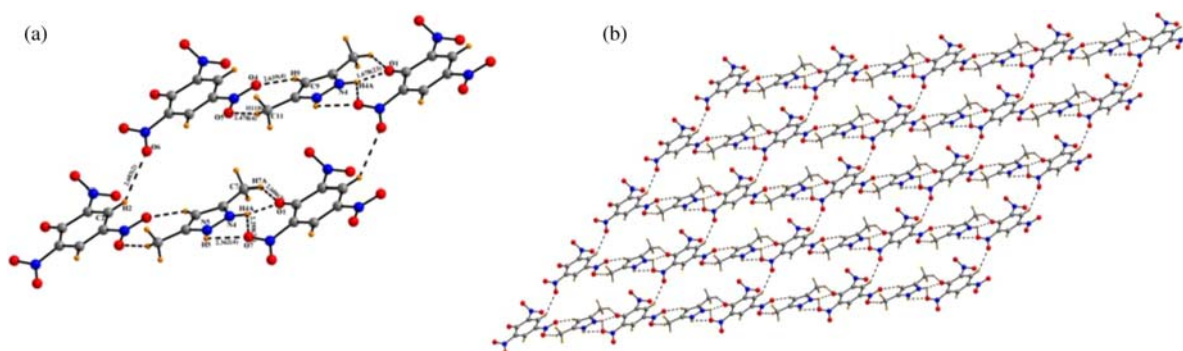


Figure 4. (a) Various non-covalent interactions and (b) Sheet like packing via N–H···O, C–H···O interactions, forming a rectangular cavity in **2**.

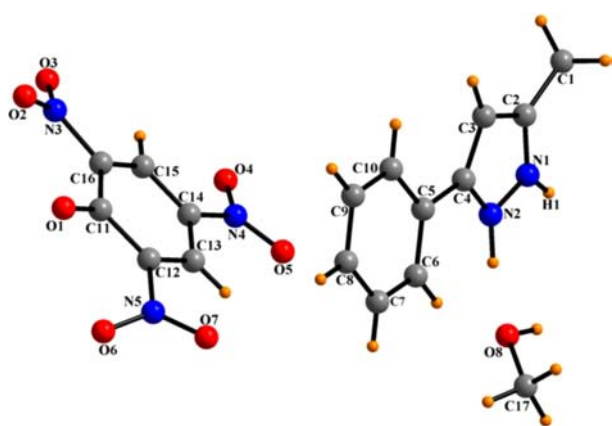


Figure 5. Molecular structure of salt **3**.

salts and the crystal structure suggests that the orientation and interaction remain almost the same from the gaseous to the solid phase (Table S2, available online). The optimised bond lengths and angles for salts **1–4** are given in Table S1 (available online), which again show that the molecules are arranged in same fashion in both solid and gaseous phases.

3.3 Thermal analysis

These salts are stable at room temperature and their thermal stability is demonstrated by a thermogravimetric (TG), derivative thermogravimetric (DTG) and differential thermal analysis (DTA). The thermoanalytical data for salts **1–4** are listed in Table 4, and the non-isothermal TG–DTA curves of salts **1–4** are shown in Figures S4–S7 (available online). Salt **1** shows two steps of decomposition. In the first step (71–205°C), one water molecule and protonated pyrazole leave out (~23.4% mass loss) which corresponds to endotherm at 159°C in DTA thermogram, while in the second step (205–279°C) one picrate ion (~72.8% mass loss) leaves out exothermically at 350°C. Beyond this temperature, the explosion of resulting mass occurs with the formation of gaseous products. The TG–

DTA thermogram for salt **2** indicates that it also undergoes two stages of decomposition. The first stage (~28.2% mass loss) corresponds to endotherm at 102°C. In this step, one molecule of 3,5-dimethylpyrazolate (92–200°C) leaves out. In the second stage (200–234°C), picrate ion leaves (~68.5% mass loss) which corresponds to exotherm at 278°C. Three steps of decomposition take place in salt **3**. In the first step, methanol molecule releases in the 101–225°C temperature range (~7.1% mass loss) which corresponds to endotherm at 162°C, while in next second and third steps, both 3-phenyl-5-methylpyrazolate and picrate ions release in 225–295°C (~52.8% mass loss) and 505–666°C (~35.9% mass loss) temperature range, respectively. The DTA peak at 281°C and 589°C is exothermic for both steps, respectively. TG curve of salt **4** exhibited three well-separated weight loss stages. In first step, acetonitrile molecule releases in 99–171°C temperature ranges (~4.6% mass loss). In second step (240–289°C), protonated Me₄bpz leaves out (~49.7% mass loss) exothermically at 293°C, while picrate ion (~45.1% mass loss) also releases (289–689°C) exothermically at 686°C in third step.

The kinetics of thermal decomposition of salts **1–4** was evaluated using 14 mechanisms based on kinetic models as given in Table S3 (available online). The set of reaction models (36) were used to analyse the isothermal TG data in the range of 200–240°C for **1–4** (Figure. 10) to calculate the E_a values for thermal decomposition, which were done in the range of decomposition/vapourisation using indigenously fabricated TG apparatus. The activation energy values are reported in Table 5. In the model-fitting method, the kinetics is analysed by choosing a ‘best-fit’ model based on the value of the correlation coefficient r close to 1. Average values 55.5, 64.3, 67.0 and 55.0 kJ mol⁻¹ have been obtained as activation energies for isothermal decomposition of salts **1–4**. The isoconversional method is known to permit estimation of activation energy independent of the model used. This method is being used to establish a relation between activation energy and extent of conversion (α) of the sample. According to Figure 11, for a particular salt, each activation energy has a

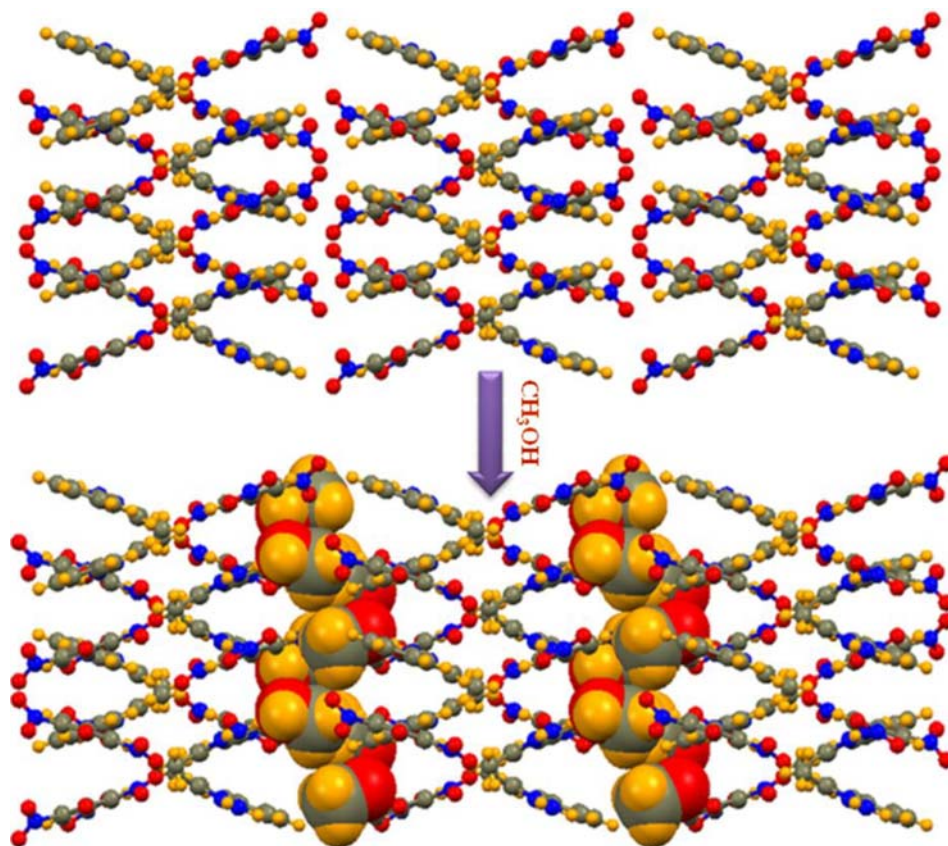


Figure 6. Host-guest complex formed due to N–H···O, C–H···O intermolecular interactions in salt **3**. (The CH₃OH molecules occupying the oval shaped cavity as guest molecules between the cross wires are represented in space-fill model).

separate value at different α . Although these salts are stable at room temperature but ignite when subjected to sudden high temperature. Further to evaluate the sensitivity of these salts, their ignition delay measurement was carried out in temperature ranges 340–380°C for salts **1–4** (Table 6). For salts **1–4**, E_a^* was determined from the slope of a plot of

$\ln(D_i)$ versus $1/T$ as shown in Figure 12. The energy of activation for ignition is 28.6, 29.3, 46.4 and 37.7 kJ mol⁻¹ for salts **1–4**, respectively. From the ignition delay measurements, it is clear that the salt **3** is highly thermal stable than **1**, **2** and **4** as it has the highest activation energy of ignition delay. The activation energy (calculated by isothermal TG) and ignition delay measurement have different values that may be due to the different temperature ranges. The OB values reported in Table 6 suggest that these salts belong to low explosives.

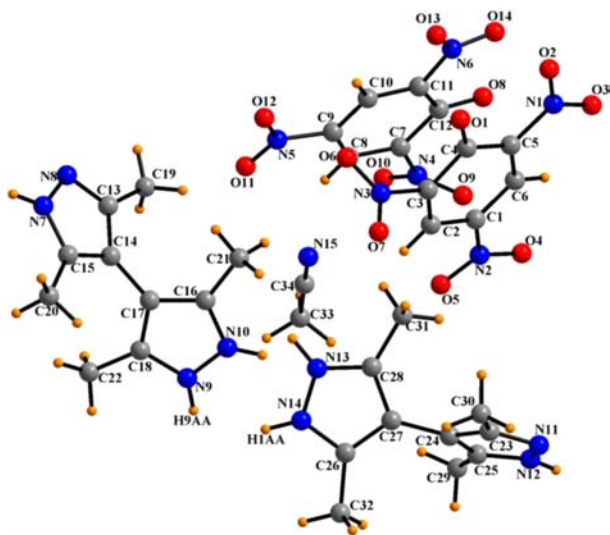


Figure 7. Molecular structure of salt **4**.

4. Conclusion

In summary, we prepared the hydrogen bonded supramolecular architecture of picric acid with different substituted pyrazole having different 3D packing views. Different factors such as variation of substituents, number and type of interactions, and the orientation of the molecules in 3D spaces are responsible for the change in the packing. Our structure analysis reveals that in salts **1–4** the host molecules self-assembled due to various types of non-covalent interactions and form different shaped cavity. On the other hand, the solvent molecules as water, methanol and acetonitrile behave as the guest molecule and occupied the cavity in salts **1**, **3** and **4**. The present study

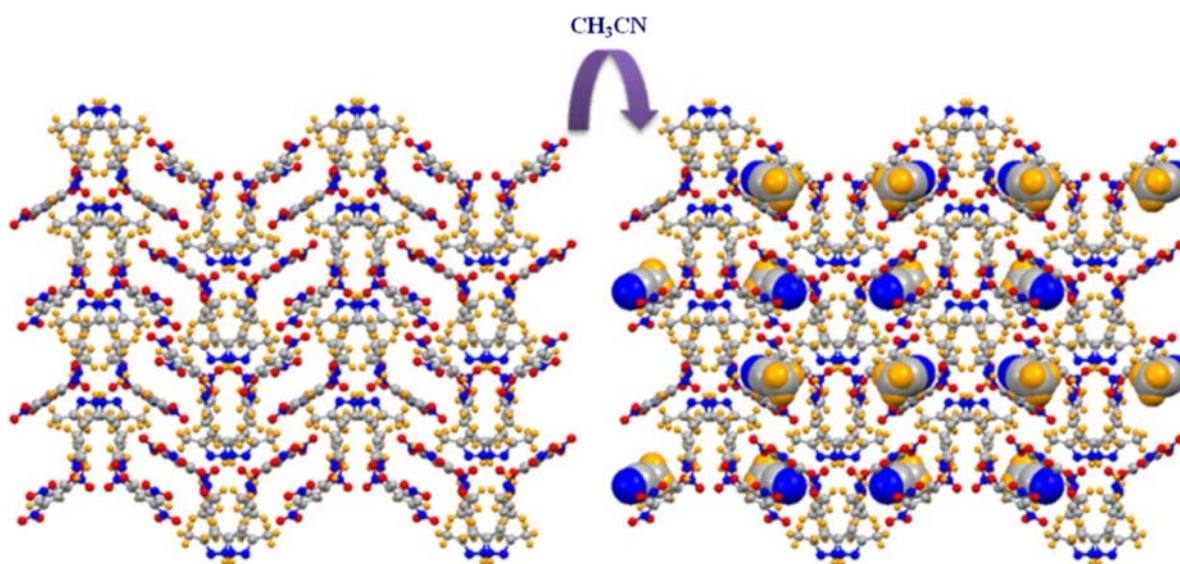


Figure 8. Host-guest complex formed due to $N-H\cdots O$, $C-H\cdots O$, $C-H\cdots N$ intermolecular interactions in salt **4**. (The CH_3CN molecules occupying the rectangular shaped cavity as guest molecules are represented in space-fill model).

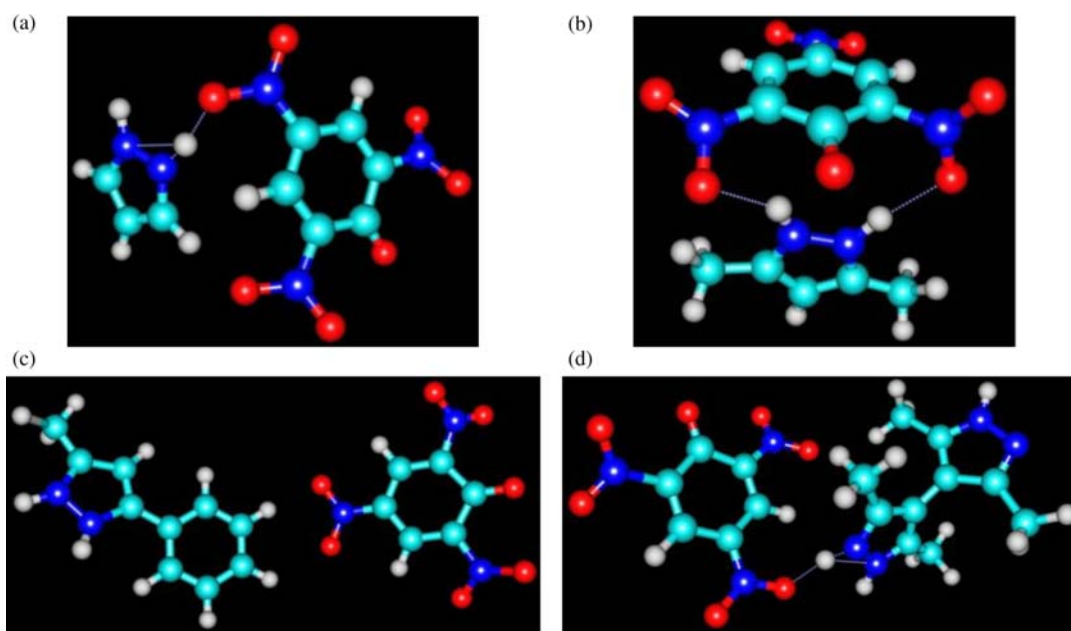


Figure 9. Optimised geometry of salts (a) **1**, (b) **2**, (c) **3** and (d) **4**.

Table 3. Hydrogen bond interaction energy (kcal/mol).

S. N	Salts	Hydrogen bond interaction energy (kcal/mol)
1.	$[2PA^- \cdot 2PzH_2^+ \cdot OH_2]$ (1)	13.39
2.	$[PA^- \cdot Pz^{Me_2}H_2^+]$ (2)	14.51
3.	$[PA^- \cdot Pz^{Ph,Me}H_2^+ \cdot CH_3OH]$ (3)	26.56
4.	$[2PA^- \cdot 2Me_4bpzH^+ \cdot CH_3CN]$ (4)	21.96

demonstrated that the variation of substituent groups on pyrazole ring plays an important role in controlling the structure of the salts. Theoretical studies also suggested that in both solid and gaseous phase, structure is same and hydrogen bond interaction energy largely depends on the functional moieties that are being involved in the interaction. From the ignition delay measurements, it is clear that the salt **3** is highly thermal stable than others as it has the highest activation energy of ignition delay.

Table 4. TG–DTA phenomenological data of salts 1–4 under air atmosphere.

Salts	Stage	TG		DTA		DTG
		T range /°C	Observed mass loss (%)	Peak temp. (°C)	Nature	Peak temp. (°C)
[2PA ⁻ ·2PzH ₂ ⁺ ·OH ₂] (1)	I	71–205	23.4	159	endo	135
	II	205–279	72.8	280	exo	268
[PA ⁻ ·Pz ^{Me2} H ₂ ⁺] (2)	I	92–200	28.2	102	endo	190
	II	200–324	68.5	278	exo	271
[PA ⁻ ·Pz ^{Ph,Me} H ₂ ⁺ ·CH ₃ OH] (3)	I	101–225	7.1	162	endo	161
	II	225–295	52.8	281	exo	275
	III	505–666	35.9	589	exo	592
[2PA ⁻ ·2Me ₄ bpzH ⁺ ·CH ₃ CN] (4)	I	99–151	4.6	154	endo	147
	II	240–289	49.7	293	exo	282
	III	289–689	45.1	686	exo	678

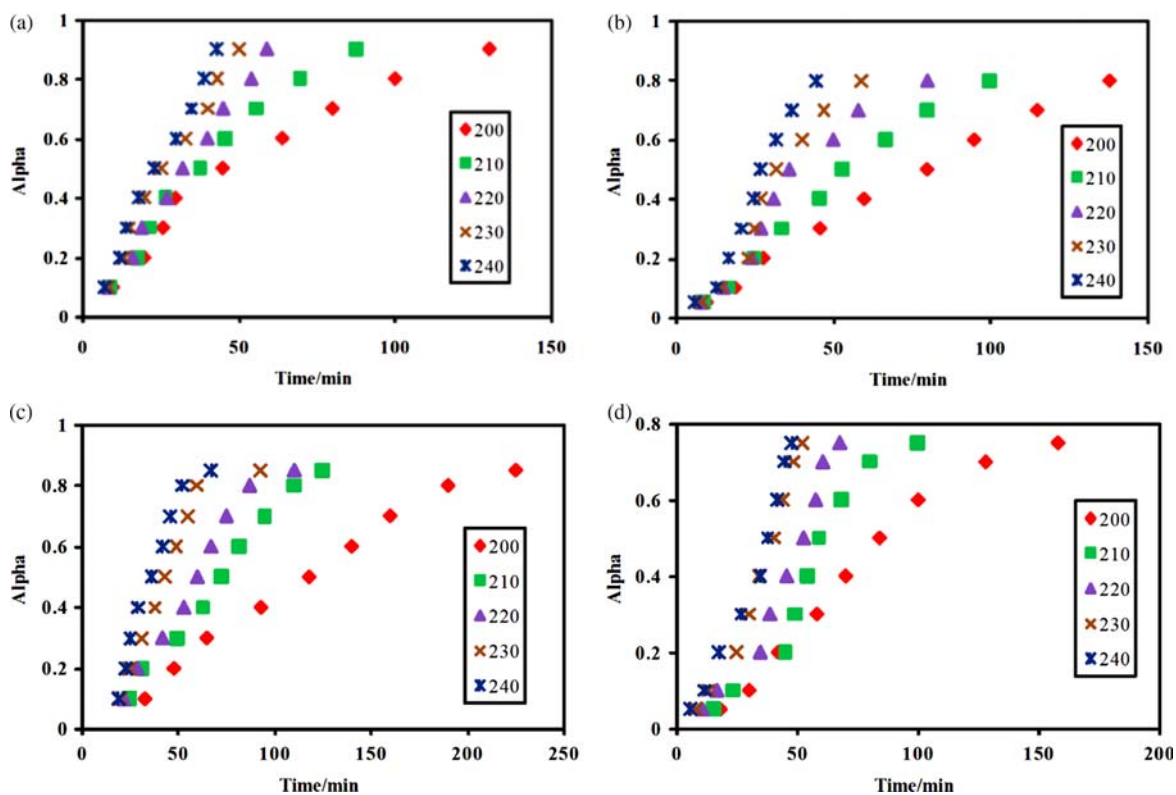
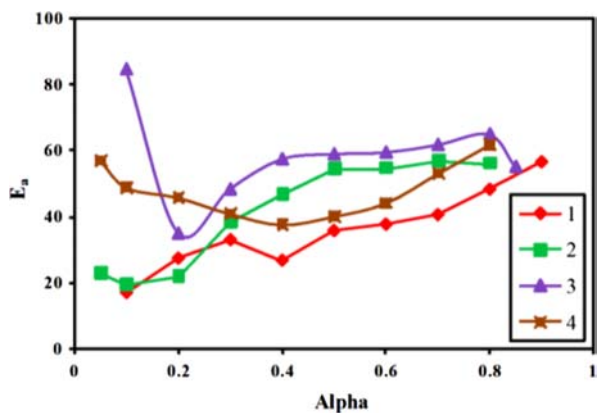
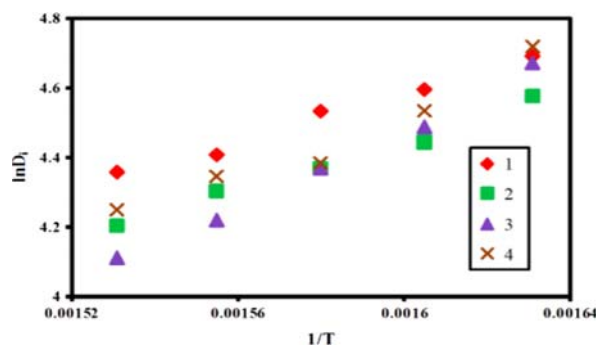


Figure 10. Isothermal TG in static air atmosphere for salts 1–4 (a) 1, (b) 2, (c) 3 and (d) 4.

Table 5. Arrhenius parameters for isothermal decomposition of salts 1–4.

Salts Model ^a	(1)		(2)		(3)		(4)	
	E_a	r	E_a	r	E_a	r	E_a	r
1	61.5	0.9718	66.0	0.9983	62.8	0.9643	60.5	0.9484
2	61.3	0.9722	65.8	0.9984	62.9	0.9650	60.2	0.9490
3	60.9	0.9728	65.4	0.9986	63.3	0.9663	59.4	0.9501
4	58.5	0.9756	64.3	0.9991	65.0	0.9728	55.0	0.9533
5	57.4	0.9765	64.1	0.9990	65.8	0.9752	53.1	0.9531
6	56.2	0.9762	64.6	0.9990	66.3	0.9764	53.9	0.9516
7	58.6	0.9750	64.6	0.9989	64.7	0.9716	57.4	0.9515
8	59.1	0.9740	65.4	0.9989	64.4	0.9702	58.1	0.9499
9	58.3	0.9757	65.1	0.9990	64.9	0.9720	57.1	0.9507
10	57.5	0.9364	64.6	0.9991	65.6	0.9743	55.0	0.9521
11	54.5	0.9754	64.7	0.9575	67.9	0.9566	50.4	0.8888
12	58.0	0.9767	64.6	0.9991	65.2	0.9732	55.6	0.9522
13	59.0	0.9737	65.9	0.9988	64.3	0.9698	59.0	0.9483
14	55.5	0.9770	64.3	0.9987	67.0	0.9784	51.2	0.9512

Note: E_a = kJ/mol.^a Enumeration of the model is as given in Table S3 (available online).Figure 11. Dependence of activation energy (E_a) on the extent of conversion (α) for salts 1–4.Figure 12. Graph of $\ln D_i$ vs $1/T$.Table 6. Activation energy for thermal ignition (E^*) and correlation coefficient (r) for salts 1–4.

Salts	D_i/s at temperature ($^{\circ}C$)					$E^*/kJmol^{-1}$ (kJ/mol)	r	OB
	340 ± 1	350 ± 1	360 ± 1	370 ± 1	380 ± 1			
(1)	109	99	93	82	78	28.58	0.9933	– 57.60
(2)	97	85	79	74	67	29.30	0.9931	– 66.17
(3)	107	89	79	68	61	46.45	0.9973	– 79.78
(4)	112	93	80	77	70	37.75	0.9742	– 71.50

5. Supporting Information Available

CCDC numbers 844776 – 844779 contain the supplementary crystallographic data (CIF) for this article. These data can be obtained free of charge from the Director, CCDC, 12 Union Road, Cambridge CB2 1EZ, UK (Fax: +44-1223-336-033; e.mail: deposit@ccdc.cam.ac.uk or [http://](http://www.ccdc.cam.ac.uk)

www.ccdc.cam.ac.uk). The additional DFT calculations and figures are available in PDF formats.

Acknowledgements

The authors gratefully acknowledge CSIR, New Delhi, India, for their financial assistance in the form of SRF to Nidhi Goel.

References

- (1) Desiraju, G.R. *Angew. Chem., Int. Ed.* **1995**, *34*, 2311.
- (2) Moulton, B.; Zaworotko, M.J. *Chem. Rev.* **2001**, *101*, 1629.
- (3) Beatty, A.M. *Cryst. Eng. Comm.* **2001**, *51*, 1.
- (4) Reger, D.L.; Debreczeni, A.; Horger, J.J.; Smith, M.D. *Cryst. Growth Des.* **2011**, *11*, 4068.
- (5) Porada, J.H.; Neudörfl, J.; Blunk, D. *Cryst. Growth Des.* **2011**, *11*, 3648.
- (6) Srinivasan, P.; Kanagasekaran, T.; Gopalakrishnan, R.; Bhagavannarayana, G.; Ramasamy, P. *Cryst. Growth Des.* **2006**, *6*, 1663.
- (7) Yamaguchi, S.; Goto, M.; Takayanagi, H.; Ogura, H. *Bull. Chem. Soc. Jpn.* **1988**, *61*, 1026.
- (8) In, Y.; Nagata, H.; Doi, M.; Ishida, T.; Wakahara, A. *Acta Crystallogr.* **1997**, *C53*, 367.
- (9) Dobrowolska, W.S.; Bator, G.; Sobczyk, L.; Grech, E.; Scheibe, J.N.; Pawlukoje, A.; Wuttke, J. *J. Mol. Struct.* **2010**, *975*, 298.
- (10) Jin, S.; Zhang, W.; Wang, D.; Gao, V.; Zhou, J.Z.; Chen, R.; Xu, X. *J. Chem. Crystallogr.* **2009**, *40*, 87.
- (11) Chandramohan, A.; Bharathikannan, R.; Kandhaswamy, M.A.; Chandrasekaran, J. *Cryst. Res. Technol.* **2008**, *43*, 93.
- (12) Yathirajan, H.S.; Narayana, B.; Swamy, M.T.; Sarojini, B.K.; Bolte, M. *Acta Crystallogr.* **2008**, *E64*, o119.
- (13) Narayana, B.; Sarojini, B.K.; Kamath, K.P.; Yathirajan, H.S.; Bolte, M. *Acta Crystallogr.* **2008**, *E64*, o117.
- (14) MacDonald, J.C.; Yigit, M.V.; Mychajlonka, K. *Cryst. Growth Des.* **2005**, *5*, 2248.
- (15) Muthamizhchelvan, C.; Saminathan, K.; Fraanje, J.; Peschar, R.; Sivakumar, K. *Anal. Sci.* **2005**, *21*, x61.
- (16) Smith, G.; Wermuth, U.D.; Healy, P.C. *Acta Crystallogr.* **2004**, *E60*, o1800.
- (17) Llamas-Saiz, A.L.; Foces-Foces, C.; Echevarría, A.; Elguero, J. *Acta Crystallogr.* **1995**, *C51*, 1401.
- (18) Infantes, L.; Foces-Foces, C.; Claramunt, R.M.; López, C.; Elguero, J. *J. Heterocycl. Chem.* **1999**, *36*, 595.
- (19) Zaderenko, P.; Gil, M.S.; López, P.; Ballesteros, P.; Fonseca, I.; Albert, A. *Acta Crystallogr.* **1997**, *B53*, 961.
- (20) Perrin, D.D.; Armarego, W.L.; Perrin, D.R. *Purification of Laboratory Chemicals*, 2nd ed. Pergamon: New York, 1980.
- (21) Puerta, D.T.; Cohen, S.M. *Inorg. Chim. Acta* **2002**, *337*, 459.
- (22) Mosby, W.L. *J. Chem. Soc.* **1957**, 3997.
- (23) Sheldrick, G.M.; University of Göttingen: Germany, 1996.
- (24) Sheldrick, G.M. *Acta Crystallogr.* **1990**, *A46*, 467.
- (25) Sheldrick, G.M. *SHELXTL-NT*; University of Göttingen: Germany, 2000.
- (26) Brandenburg, K. *DIAMOND*; Crystal Impact GbR: Bonn, Germany, 2000.
- (27) MERCURY, Cambridge Crystallographic Data Centre. 12 Union Road, Cambridge CB2 1EZ: UK. Available from: Website: <http://www.ccdc.cam.ac.uk/>.
- (28) Gaussian 03, *Rev. C.02*; Gaussian, Inc. Wallingford CT, 2004.
- (29) Hariharan, P.C.; Pople, J.A. *Theo. Chem. Acta* **1972**, *28*, 213.
- (30) Singh, G.; Singh, R.R. *Res. Ind.* **1978**, *23*, 92.
- (31) Singh, G.; Vasudeva, S.K.; Kapoor, I.P.S. *Indian J. Tech.* **1991**, *29*, 589.
- (32) Zinn, J.; Rogers, R.N. *J. Phys. Chem.* **1962**, *66*, 2646.
- (33) Semenov, N. *Chemical Kinetics: Chain Reactions*; Clarendon Press: Oxford, Chapter 18, 1935.
- (34) Freeman, E.S.; Gorden, S. *J. Phys. Chem.* **1956**, *60*, 867.
- (35) Martin, A.R.; Yallop, H.J. *Trans Faraday Soc.* **1958**, *54*, 257.
- (36) Brown, M.E.; Dollimore, D.; Galway, A.K. Reaction in the Solid State. *Comprehensive Chemical Kinetics*; Elsevier: Amsterdam, 1960; Vol. 22, pp. 1–340.
- (37) Singh, G.; Felix, P.S.; Pandey, D.K. *Thermochim. Acta* **2004**, *411*, 61.
- (38) Ghazaryan, V.V.; Fleck, M.; Petrosyan, A.M. *Spectrochim. Acta* **2011**, *A78*, 128.
- (39) Ikeda, C.; Nagahara, N.; Motegi, E.; Yoshioka, N.; Inoue, H. *Chem. Commun.* **1999**, *43*, 1759.
- (40) Silverstein, R.M.; Bassler, G.C.; Morrill, T.C. *Spectrometric Identification of Organic Compounds*, 5th ed. Wiley: New York, 1991.

ERRATUM

The version of this article, originally published online on 23 April 2012, has been corrected to include missing figures.

Taylor & Francis wishes to apologise for this oversight.